

DESIGN OF A HIGH PEAK POWER THz FEL DRIVEN BY A PITZ-LIKE PHOTOINJECTOR

D. Xu*, N. Aftab, A. Aksoy, M. Krasilnikov, B. Li, X. Li, S. Pakluea
Deutsches Elektronen-Synchrotron DESY, Zeuthen, Germany

Abstract

The Photo Injector Test Facility at DESY in Zeuthen (PITZ) is developing a THz free electron laser (FEL) as a potential source for pump-probe experiments at the European XFEL. In this work, we present a simulation study for an ideal THz FEL facility driven by a PITZ-like injector. The ideal machine features a beam energy of up to 45 MeV, two APPLE-II undulators, and a bunch compressor with tunable R_{56} . A parameter study of the FEL performance is carried out to identify favorable electron beam parameter regimes. Start-to-end (S2E) simulations with multi-objective genetic algorithm optimization of the injector are then performed to evaluate the achievable THz radiation performance. The S2E simulations yield a THz pulse energy of $\sim 800 \mu\text{J}$ at 10 THz in self-amplified spontaneous emission mode with a 1 nC bunch, and $\sim 35 \mu\text{J}$ with an rms pulse length of $\sim 1.5 \text{ ps}$ at 1 THz in superradiance mode with a 200 pC bunch.

INTRODUCTION

The European XFEL generates ultrashort X-ray pulses suitable for pump-probe experiments, in which an optical or THz pump pulse excites a sample and a time-delayed X-ray probe pulse captures the sample dynamics. A high-peak-power THz source synchronized with the XFEL would significantly expand the capabilities of such experiments. The Photo Injector Test Facility at DESY in Zeuthen (PITZ) is developing a THz free-electron laser (FEL) to serve as such a source.

Currently, pulse energies exceeding $100 \mu\text{J}$ at 3 THz have been generated in a proof-of-principle experiment using the LCLS-I undulator together with a 17 MeV/c electron beam with bunch charges of up to 2.5 nC from the PITZ injector [1]. These results confirm the viability of the PITZ-based THz FEL concept, but full performance was limited by the multipurpose nature of the facility, which is not optimized for THz generation.

To explore the full potential of a dedicated THz FEL, we present a simulation study of an ideal machine — a facility fully optimized for THz generation driven by a PITZ-like photoinjector.

Four operational cases are considered: self-amplified spontaneous emission (SASE) at 1 THz and 10 THz, and superradiance (SR) at 1 THz and 0.3 THz, corresponding to the four marked points in Fig. 1(b). A parameter study of the FEL performance is first carried out to identify favorable beam-parameter regimes for each case. The results inform the optimization objectives of the subsequent start-to-end (S2E) simulations, in which the injector is optimized using

a multi-objective genetic algorithm (MOGA) and the beam is tracked through the bunch compressor and the undulator.

IDEAL MACHINE LAYOUT

Compared to the existing PITZ beamline, the ideal machine incorporates three major upgrades. First, the beam energy is increased to up to 45 MeV to suppress space-charge effects and enable wide frequency tunability. Second, two APPLE-II undulators cover complementary frequency ranges — SR at 0.1–1 THz and SASE at 1–30 THz. Third, a bunch compressor with tunable R_{56} provides flexible control of the bunch length and peak current. The undulators of the ideal machine are configured with helical polarization, which provides higher FEL gain and power as well as symmetric focusing of the electron beam, while the APPLE-II design retains the flexibility of variable polarization. Key parameters of the existing and ideal beamlines are summarized in Table 1.

Table 1: Comparison of Key Parameters Between the Existing PITZ Beamline and the Ideal Machine

Parameter	PITZ	IM SR	IM SASE
Beam energy	$\leq 22 \text{ MeV}$	$\leq 45 \text{ MeV}$	
Und. type	LCLS-I	APPLE-II	
Polarization	horizontal	tunable	
λ_u (mm)	30	130	65
Periods	113	5 to 10	60
K	3.49	2.7 to 6.8	0.7 to 2.9
Freq. (THz)	1 to 5	0.1 to 1	1 to 30
R_{56}	fixed	tunable	

*IM = ideal machine

The undulator design follows the APPLE-II parametrization in Ref. [2], which gives the peak magnetic field B_0 in helical mode as

$$B_0 = a \exp\left(-b \frac{g}{\lambda_u} + c \left(\frac{g}{\lambda_u}\right)^2\right), \quad (1)$$

where g is the undulator gap and λ_u the period length, with $a = 1.54$, $b = 4.46$, $c = 0.43$ for both undulators. From B_0 , the undulator parameter K and the FEL wavelength λ_s are obtained as

$$K = \frac{eB_0\lambda_u}{2\pi m_e c}, \quad (2)$$

$$\lambda_s = \frac{\lambda_u}{2\gamma^2} (1 + K_{\text{rms}}^2), \quad (3)$$

where $K_{\text{rms}} = K$ for a helical undulator. The resulting K and λ_s curves are shown in Fig. 1.

* duo.xu@desy.de

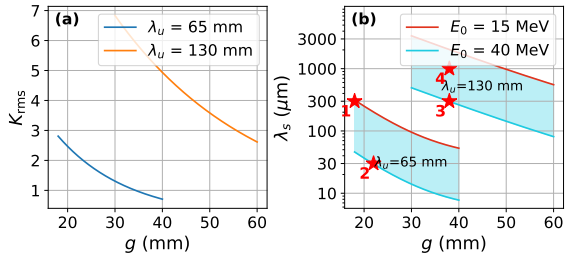


Figure 1: Undulator parameters as functions of the gap for the two APPLE-II undulators: (a) undulator parameter K , and (b) FEL wavelength λ_s for beam energies from 15 MeV to 40 MeV.

FEL PARAMETER STUDY

Electron Bunch Parameters at Undulator Entrance

The electron bunches are modeled with a four-dimensional Gaussian transverse phase-space distribution and an inverted parabola longitudinal current profile. The following parameters are held fixed throughout the study: the normalized emittances $\epsilon_{x,n} = \epsilon_{y,n} = 5 \mu\text{m}$, the uncorrelated energy spread $\sigma_E^{\text{uncor}} = 10 \text{ keV}$, and the Twiss parameter $\alpha_{x0} = \alpha_{y0} = 0$.

The scanned parameters are the bunch charge Q , the peak current I_p , the correlated energy spread σ_E^{cor} , and the initial beta function at the undulator entrance. The beta function is expressed in units of the equilibrium beta function β_{eq} , which follows from the undulator natural focusing:

$$\beta_{\text{eq}} = \frac{1}{\sqrt{k_1}}, \quad (4)$$

$$k_1 = \frac{2\pi^2 K^2}{\gamma^2 \lambda_u^2}, \quad (5)$$

where k_1 is the natural focusing strength of the undulator [3]. The horizontal and vertical beta functions are coupled by the equilibrium condition $\beta_{x0} \beta_{y0} = \beta_{\text{eq}}^2$, so that $\beta_{x0}/\beta_{\text{eq}}$ serves as a single independent scanning variable. The condition $\beta_{x0} = \beta_{\text{eq}}$ minimizes the average beta function — and hence the average transverse beam size — along the undulator.

Parameter Scan Results

For the SASE cases, the scanned parameter ranges are: bunch charges $Q = 1, 2, \text{ and } 3 \text{ nC}$, peak current $I_p = 100 \text{ A to } 800 \text{ A}$ in steps of 100 A, $\beta_{x0}/\beta_{\text{eq}}$ from 1 to 50, and correlated energy spread σ_E^{cor} from $-500 \text{ keV to } 0$ (Case 1) and from 0 to 1000 keV (Case 2). For each parameter set the THz pulse energy is evaluated via GENESIS 1.3, producing a heat map over the $\sigma_E^{\text{cor}} - \beta_{x0}/\beta_{\text{eq}}$ plane. For brevity, only a subset of the heat maps ($Q = 1 \text{ nC}$, $I_p = 200 \text{ A}$, 400 A and 600 A) is displayed in Figs. 2 and 3. The optimal pulse energy (maximized over σ_E^{cor} and $\beta_{x0}/\beta_{\text{eq}}$) as a function of I_p for each Q is summarized in Fig. 4.

In Case 1 (15.3 MeV), space-charge effects are significant: the pulse energy saturates with increasing I_p at thresholds of $\sim 300 \text{ A}$, 500 A and 600 A for $Q = 1, 2, \text{ and } 3 \text{ nC}$, and the

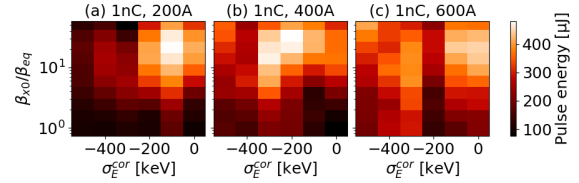


Figure 2: Heat maps of THz pulse energy for Case 1 (1 THz SASE) at $Q = 1 \text{ nC}$.

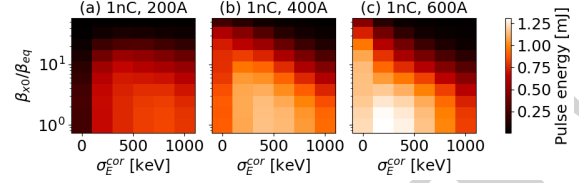


Figure 3: Heat maps of THz pulse energy for Case 2 (10 THz SASE) at $Q = 1 \text{ nC}$.

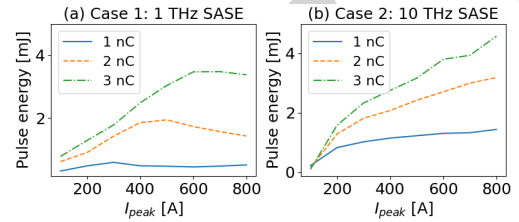


Figure 4: Optimal THz pulse energy (maximized over σ_E^{cor} and $\beta_{x0}/\beta_{\text{eq}}$) as a function of I_p for Cases 1 and 2.

optimum occurs at negative σ_E^{cor} and $\beta_{x0} \gg \beta_{\text{eq}}$, consistent with a negative chirp counteracting the space-charge-driven bunch lengthening and a larger transverse size reducing the charge density. In Case 2 (39.7 MeV) space-charge is largely suppressed: no saturation is observed, and the optimum shifts to positive σ_E^{cor} at $\beta_{x0} \approx \beta_{\text{eq}}$.

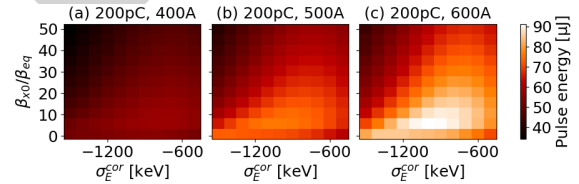


Figure 5: Heat maps of THz pulse energy for Case 3 (1 THz SR) at $Q = 200 \text{ pC}$.

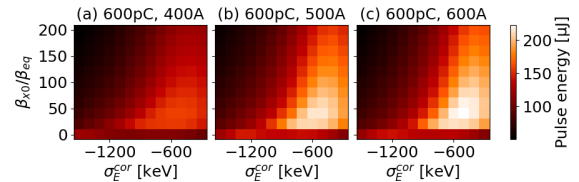


Figure 6: Heat maps of THz pulse energy for Case 4 (0.3 THz SR) at $Q = 600 \text{ pC}$.

The SR results are shown in Figs. 5 and 6. All SR simulations use the minimum of 5 undulator periods listed in Table 1. In both cases the bunch length is shorter than one FEL wavelength and space-charge effects are therefore significant. As with the low-energy SASE case, the optimum

occurs at negative σ_E^{cor} and $\beta_{x0} > \beta_{\text{eq}}$, with $\beta_{x0}/\beta_{\text{eq}} \approx 5$ for Case 3 and several tens for Case 4.

START-TO-END SIMULATIONS

The S2E simulation chain comprises beam generation and acceleration with ASTRA, bunch compression with Ocelot, and FEL simulation with GENESIS 1.3. Two working points are selected from the parameter study as S2E targets: Case 2 (1 nC, 400 A, 10 THz SASE) and Case 3 (200 pC, 400 A, 1 THz SR).

The photoinjector layout assumes the existing PITZ gun, solenoid, and booster cavity, followed by a second accelerating cavity of the same type. Optimization is performed with a MOGA. The bunch charge is fixed per case, and the laser is modeled as a truncated Gaussian in the transverse plane (truncation determined by the beam shaping aperture, BSA) with a Gaussian temporal profile. Table 2 lists the independent variables and their ranges. The MOGA optimizes three objectives: the longitudinal phase-space linearity (quantified by a non-linearity factor), the peak current, and the correlated energy spread.

Table 2: MOGA Independent Variables and Their Ranges

Variable	Range
Laser FWHM	5 to 20 ps
BSA (Case 2)	2 to 4 mm
BSA (Case 3)	0.7 to 4 mm
Gun phase	-20 to 10°
Acc. cavity phases	-15 to 15°
Solenoid current	340 to 400 A

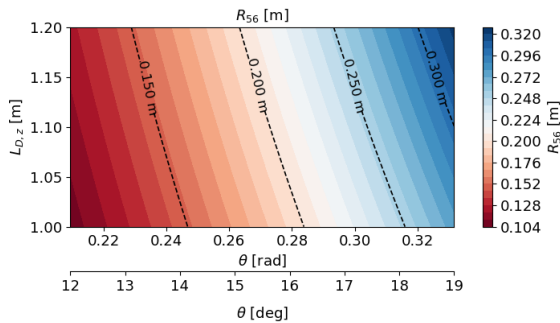


Figure 7: Analytically calculated R_{56} as a function of z -projected drift length $L_{D,z}$ and bend angle θ .

For each case, one solution from the MOGA optimization that prioritizes longitudinal phase-space linearity is selected. Given the pre-compression bunch parameters from the injector and the target peak current at the undulator entrance, the required R_{56} of the bunch compressor is determined from linear compression theory. Case 2 targets a positive σ_E^{cor} , corresponding to an over-compression condition, while Case 3 targets a negative value, corresponding to under-compression. The resulting R_{56} is ~ 0.25 m for Case 2 and ~ 0.15 m for Case 3. Figure 7 shows the R_{56} values obtained analytically as a function of z -projected drift length $L_{D,z}$ and bend angle θ for both cases.

The selected injector solutions are tracked through the chicane and the final FEL performance is evaluated with GENESIS 1.3. Figure 8 presents the S2E results for Cases 2 and 3. Subplots (a, c, e) correspond to Case 2 (10 THz SASE) and (b, d, f) to Case 3 (1 THz SR).

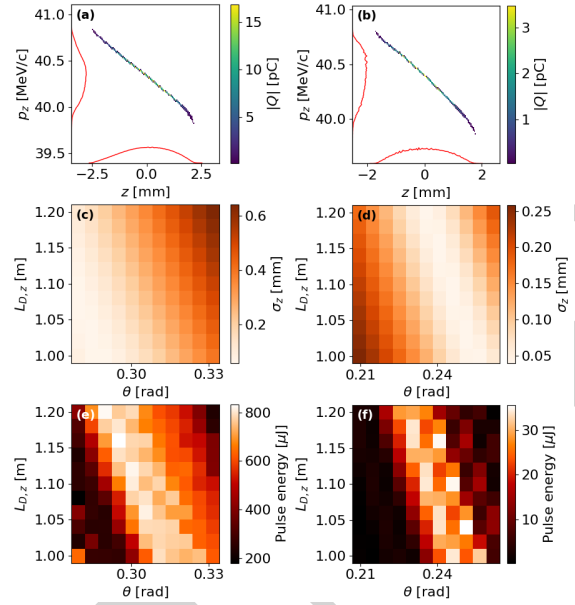


Figure 8: S2E simulation results: (a, b) longitudinal phase space before compression; (c, d) σ_z after compression; (e, f) THz pulse energy, with (c–f) scanned over $L_{D,z}$ and θ .

CONCLUSION

A simulation study of an ideal THz FEL facility driven by a PITZ-like photoinjector has been carried out. The ideal machine features a beam energy of up to 45 MeV, two helical APPLE-II undulators covering 0.1–30 THz, and a bunch compressor with tunable R_{56} . The parameter study shows that at low beam energy and for short SR bunches, the optimal THz pulse energy is obtained with negative correlated energy spread and $\beta_{x0} \gg \beta_{\text{eq}}$, whereas at higher SASE energies the optimum shifts to a positive energy chirp at $\beta_{x0} \approx \beta_{\text{eq}}$.

S2E simulations with MOGA-optimized injector settings yield a THz pulse energy of ~ 800 μJ at 10 THz in SASE mode and ~ 35 μJ with an rms pulse length of ~ 1.5 ps at 1 THz in SR mode.

REFERENCES

- [1] M. Krasilnikov *et al.*, “First high peak and average power single-pass THz free-electron laser in operation”, *Phys. Rev. Accel. Beams*, vol. 28, no. 3, p. 030701, 2025. doi:10.1103/PhysRevAccelBeams.28.030701
- [2] P. Boonpornprasert, “Investigations on the capabilities of THz production at the PITZ facility”, Ph.D. thesis, Universität Hamburg, Hamburg, Germany, 2020.
- [3] K.-J. Kim, Z. Huang, and R. Lindberg, *Synchrotron radiation and free-electron lasers*. Cambridge, UK: Cambridge University Press, 2017. doi:10.1017/9781316677377